

Are all Equations of State in Neutron Stars born alike?

Eva Lope Oter^{a,*}

^a*Departamento de Física Teórica & IPARCOS[†],
Universidad Complutense de Madrid, E-28040 Madrid, Spain.*

E-mail: mariaevl@ucm.es

We have recently provided the generic band of equations of state for matter at attainable densities in zero- and finite-temperature neutron stars restricted only by hadronic physics and fundamental principles, which are crucial for testing General Relativity and theories beyond it. We also characterize any first-order phase transitions therein by the specific latent heat, which we have systematically explored with these EoS for different interpolations. In addition, we used these GR-independent equations of state to constrain the quadratic Palatini gravity $f(\mathcal{R})$. In this work, we incorporate an EoS based on no potential, rather directly from nucleon scattering data [1] for pure neutron matter (PNM) at zero temperature and very low densities by interpolation up to known higher-density physics, applying causality, monotonicity and thermal consistency, in two steps. We use a first interpolation between the uncertainty band obtained for PNM and the saturation density, constrained by nuclear experiments. Then, we use a second interpolation between this band and the high-density perturbative QCD regime and so we cover number densities in the range $10^{-8} \leq n \leq 7 \text{ fm}^{-3}$.

10th International Conference on Quarks and Nuclear Physics (QNP2024)

8-12 July, 2024

Barcelona, Spain

*Speaker

[†]Work supported by grant PID2022-137003NB-I00 of the Spanish MCIN/AEI /10.13039/501100011033/ and FEDER. Thanks also to my collaborators J. A. Oller and J. M. Alarcón.

1. Introduction

Neutron stars (NS) are ideal laboratories to study ultra-dense matter described by the equation of state (EoS), which becomes the main point of contact between macroscopic astrophysical studies and microscopic nuclear and particle physics research. In previous work, we have provided generic EoS bands at neutron star densities for cold matter [2], based on the state-of-the-art results from Chiral Effective Theories and perturbative Quantum Chromodynamic regime (pQCD), and we have further extended this work to finite temperatures [3]. These EoS's are constrained only by inputs from hadron physics and fundamental principles, without feedback from neutron stars observations and without relying on General Relativity, in order to be used to test theories of modified gravity and Beyond Standard Model physics in NS [4, 5]. We are also interested in the the question of whether NS contain quark matter in their interiors, or whether they undergo first-order phase transitions to some form of exotic matter. A way to quantify such first-order phase transition is by the matter's latent heat, which we have explored with these EoS for different interpolations [6].

This proceeding is a summary of work carried out in [7] and incorporates, as a key aspect, an EoS for pure PNM at zero temperature and very low densities directly expressed in terms of the nucleon scattering data [1], i.e. phase shifts and mixing angles and, therefore, it is a renormalized result without any regulator dependence, like a cutoff. This EoS at low number density is interpolated up to pQCD regime, applying causality, monotonicity and thermal consistency [8], in two steps. First, by interpolating between the uncertainty band resulting for the EoS [1] for PNM and saturation density, constrained by nuclear experimental data regarding the values of the symmetry energy and its slope [9, 10]. In the second step, we use another interpolation between this first band and the high-density pQCD regime [11], so we cover a whole range of baryon densities up to around 7 fm^{-3} .

2. Methodology

We start from the results for the energy per nucleon (E/A) obtained in [1] for $0 \leq n \leq 1.15 \times 10^{-3} \text{ fm}^{-3}$. We call n_L this upper value $n \approx 0.015 \text{ fm}^{-3} \approx 0.1 n_s$.

The EoS (pressure P vs energy density ε) of pure neutron matter is extracted from the knowledge of E/A as a function of n , by using the relations ($T = 0$)

$$\varepsilon = n \left(M_N + \frac{E}{A} \right), \quad (1)$$

$$P = n^2 \frac{d(E/A)}{dn} \quad (2)$$

where M_N is the nucleon mass.

Reciprocally, for each point of the EoS with $P(\varepsilon)$ assumed to be known, we obtain the corresponding values of n and E/A by using a discretized version of Eqs. (1) and (2), with the use of dense enough partitions:

$$n_{i+1} = \frac{\varepsilon_{i+1}}{M_N + (E/A)_{i+1}} \quad (3)$$

$$P_i = n_i^2 \frac{(E/A)_{i+1} - (E/A)_{i-1}}{n_{i+1} - n_{i-1}}. \quad (4)$$

These two equations are employed to solve for $(E/A)_{i+1}$ and n_{i+1} given the earlier two points i and $i - 1$, and having at hand $P(\varepsilon)$.

Furthermore, from the grand potential ensemble we calculate the baryon chemical potential μ for each point using the Euler equation

$$\mu_i = \frac{\varepsilon_i + P_i}{n_i}. \quad (5)$$

2.1 Interpolation process

Starting from the obtained values for $(\varepsilon, P, E/A, n, \mu)$ in the low-density region, we interpolate to higher densities using the interpolation procedure developed in [2]. With this method, the first step is to establish the allowed region based on the conditions of causality and monotonic behavior, which imply $0 \leq c_s^2 \leq 1$.

The next step is to construct a grid of candidate points (ε, P) (typically 1000×1000) inside this allowed region. We construct the EoS selecting a value of P of the grid for each ε value by slowly increasing the slope at the beginning of the grid, and accelerating the slope growth with the energy density with varying values for each EoS, until the maximum slope $c_s^2 \leq 1$ is obtained, while ensuring the principles of stability and causality. We also account for possible phase transitions (PTs) by increasing ε while $P(\varepsilon)$ is held fixed. Moreover, we also calculate for each point of the EoS the value of μ by means Eqs. (3)–(5), ensuring the thermodynamic consistency principle and the causality of speed of sound in the (n, μ) plane. In addition, in each interpolation, we display the bands related to the integral constraints [8], applied in this reference to the maximum and minimum $P(\varepsilon)$ values of the high matching band with pQCD.

In this way, we carry out two interpolations: *i)* From the upper limit of applicability of the EoS [1] in density, n_L , up to the saturation density n_s . *ii)* From n_s up to the pQCD limit of around $40n_s$, with a highest chemical potential $\mu_H = 2600 \pm 8$ MeV [8]. For *i)*, we restrict the information at n_s from experimental information on nuclear reactions; for *ii)*, the constraints come by requiring the reproduction of the pQCD limiting values. Next, we consider two cases, one where we do not include constraints from values obtained from astrophysical observables, and the other one where we include experimental data from astrophysics on neutron stars.

2.2 First interpolation, $n_s \geq n \geq n_L$

For the first interpolation, we constrain the EoS at $n = n_s$ from neutron skin measurements in ^{208}Pb by PREX-II [9] and ^{48}Ca by CREX [10] experiments, leading to values for the symmetry energy, S_0 , and its slope, L , at $n = n_s$. Here, the symmetry energy as a function of density is defined as $E_{\text{sym}}(n) = (E/A)_{\text{PNM}}(n) - (E/A)_{\text{SNM}}(n)$, and its slope $L_{\text{sym}}(n) = 3n\partial E_{\text{sym}}(n)/\partial n$. In the following, we denote by $S_0 = E_{\text{sym}}(n_s)$ and $L = L_{\text{sym}}(n_s)$.

From PREX-II [9] Ref. [12] deduces the values:

$$S_0 = 38.1 \pm 4.7 \text{ MeV} \quad (6)$$

$$L = 106 \pm 37 \text{ MeV}. \quad (7)$$

In turn, Ref. [13] from the CREX experiment [10] distinguishes between two scenarios and gives two possible largely different values for L_{sym} :

$$\begin{aligned} \text{Scenario 1: } & L = 110 \pm 40 \text{ MeV} , \\ \text{Scenario 2: } & L = 19 \pm 19 \text{ MeV} , \end{aligned} \tag{8}$$

not providing any independent value for S_0 . The scenario 1 value for L is compatible with Eq. (7).

Taking into account that at the equilibrium $P_{\text{SNM}}(n_s) = 0$, and the phenomenological values $(E/A)_{\text{SNM}}(n_s) = -16.0 \pm 0.5 \text{ MeV}$ and $n_s = 0.16 \pm 0.01 \text{ fm}^{-3}$, $(E/A)_{\text{PNM}}(n_s)$ and $P_{\text{PNM}}(n_s)$ can be restricted within experimentally established intervals. Thus, $(E/A)_{\text{PNM}}(n_s) \in (16.9, 27.3) \text{ MeV}$ following Eq. (6), but limiting $P_{\text{PNM}}(n_s)$ is more complicated, due to the difficulty of selecting a minimum value of L from CREX measurements (as reflected in Eq. (8)). For the maximum value $L_{\text{sym}}(n_s) = 143 \text{ MeV}$ in Eq. (7), the pressure at saturation density is $P_{\text{PNM}}(n_s) = 7.62 \text{ MeV/fm}^3$. By the Euler relation Eq. (5) these values give us the largest limit for a $\mu_H = 1014.5 \text{ MeV}$ used in the construction of the allowed regions within the (ε, p) plane following Ref. [8]. For the minimum value, we first select the lowest central value of [13] $L_{\text{sym}} = 19 \text{ MeV}$ in Eq. (8), that implies $P_{\text{PNM}}(n_s) \approx 1.01 \text{ MeV/fm}^3$. Finally, the incompatibility between PREX and CREX data in establishing a lower bound for L has led us to constraint E/A from below [14]. In this model, the energy per particle of a unitary Fermi gas of neutrons $(E/A)_{\text{UG}}$ is taken as a lower bound [14] for E/A in PNM. The resulting expression for $(E/A)_{\text{UG}}$ is universal and given by $(E/A)_{\text{UG}} = \xi(E/A)_F$, where ξ is the Bertsch parameter, $\xi = 0.370(5)(8)$ [1] and $(E/A)_F$ is E/A for a free Fermi gas. By applying Eq. (2) we then have the values $(E/A)_{\text{UG}}(n_s) = 12.7 \pm 0.3 \text{ MeV}$, $\varepsilon_{\text{UG}}(n_s) = 152.46 \pm 0.05 \text{ MeV/fm}^3$, $P_{\text{UG}}(n_s) = 1.33 \pm 0.04 \text{ MeV/fm}^3$ and $L_{\text{UG}} = 24.9 \pm 0.7 \text{ MeV}$. By applying Eq. (5) these values imply a chemical potential at n_s equal to $\mu_H = 960.6 \pm 0.6 \text{ MeV}$. This chemical potential is the smallest limit for a μ_H to be used in the construction of allowed regions of EoS in the (ε, p) plane from Ref. [8].

2.3 Second interpolation for higher densities, $n > n_s$

For the second extrapolation up to very high densities, the EoS can also be computed directly from the fundamental theory of QCD. This theory becomes perturbative at asymptotically high energies, implying a limit to the pressure, energy density, and baryon chemical potential at the pQCD matching point. The partial N³LO pQCD results of [11] shows that this regime is valid at $\mu_{p\text{QCD}} = 2.6 \text{ GeV}$ and these results still depend on the scale $X = 3\bar{\Lambda}/\mu$, with $\bar{\Lambda}$ the $\overline{\text{MS}}$ renormalization scale [8]. All the points of the EoS can be connected to the pQCD values, $(\mu_{p\text{QCD}}, \varepsilon_{p\text{QCD}}, P_{p\text{QCD}})$, by causal, stable and thermodynamically consistent interpolation at any point inside the band corresponding to $\mu_{p\text{QCD}} = 2.6 \text{ GeV}$, which we call μ_H , and the renormalization scale $X \in [1, 4]$ [8, 11], where $P \in [2330, 4380] \text{ MeV/fm}^3$.

Another key parameter to take into account to match with pQCD is the so-called critical chemical potential [8], μ_c , that corresponds to the pressure at the intersection point in the (n, μ) plane between the causal lines and the lower boundary of the branch connecting with pQCD at μ_H . Considering maximum $c_s^2 \leq 1$, this upper value cannot be held for chemical potentials $\mu \geq \mu_c$ in order to enter pQCD with $\mu_H = 2.6 \text{ GeV}$. Thus, we maintain the maximum velocity until we reach

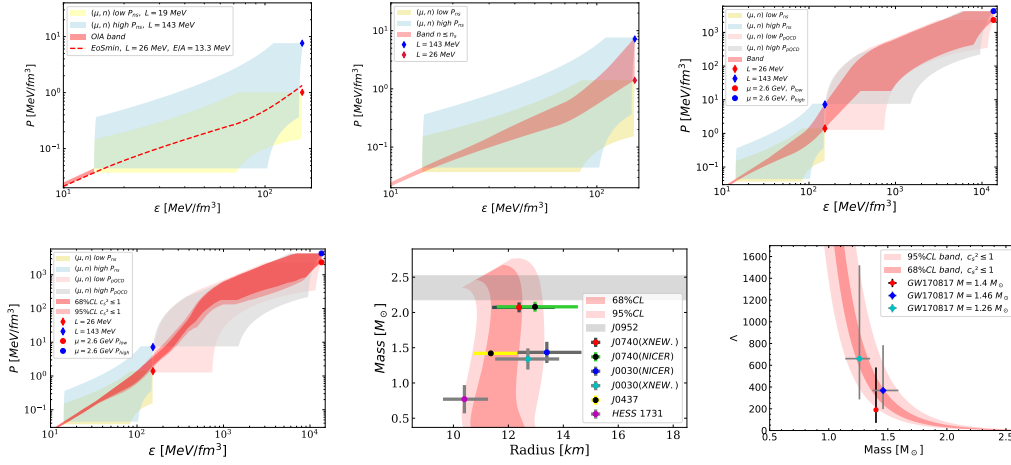


Figure 1: **Top left:** Bounding areas of validity for PNM EoS by extrapolating the EoS of Ref. [1] (reddish band) from n_L up to n_s , taking as minimum value of $L=19$ MeV. **Top center:** The same bounding bands as in the top left are shown but now the red diamond is fixed from the red dashed line. The resulting band of EoS's from the extrapolation up to n_s is the narrower red area. **Top right:** Band obtained by interpolation from low to high densities, limited only by causality and thermodynamical consistency, pQCD and from measurements of nuclear parameters. **Bottom left:** (ϵ, p) bands constrained from astrophysical observables at 68% CL (red) and 95% CL (pink) for $0 \leq c_s^2 \leq 1$. **Bottom center:** Mass-Radius diagrams for the EoS bands on the left. **Bottom right:** Tidal deformability-Mass relation for the EoS bands on the left.

a potential $\mu_0 < \mu_c = 2250$ MeV, obtaining then a value of $n(\mu_0)$ less than or equal to the central density point in the star. At this point, we link to pQCD by performing a long PT to the energy density value that allows reaching the pQCD band with a slope $c_s^2 \leq 1/3$. Other possibilities are also explored as, for example, instead of such a long PT we also allow a shorter one followed by an increase in $c_s^2 \leq 1$, and then repeating this process a few times. Furthermore, the EoS is also constrained by forbidding a PT below $2.5n_s$ [15].

3. Results and conclusions

Regarding the interpolation up to n_s , the EoS's corresponding to the lower and upper limit points of the integral constraints for the pressure at n_s ($P_s = 1.01$ MeV/fm³ or $L_{\text{sym}} = 19$ MeV) and 7.62 MeV/fm³ or $L_{\text{sym}} = 143$ MeV) are shown in the top left of Fig. 1 by the palish yellow and blue areas, respectively. Growing the EoS through the grid points, we find that the minimum EoS (red dashed line) compatible with $(E/A)_{UG}$ presents $P_s = 1.4$ MeV/fm³ at n_s , giving $L = 26.4$ MeV and $E/A = 13.3$ MeV. This value, in accordance with the UG conjecture, is smaller than the interval $(E/A)_{\text{PNM}}(n_s) \in (16.9, 27.3)$ MeV given in Eq. (6) from the phenomenological values of S_0 , L , $(E/A)_{\text{SNM}}(n_s)$ and n_s there discussed. Finally, we take $P(n_s)$ from the red dashed line in Fig. 1, the generated EoS closest to the UG results, as the lower limit at n_s , and do the interpolation matching at n_s within the extreme values $P_{\text{high}} = 7.62$ MeV/fm³ and $P_{\text{low}} = 1.41$ MeV/fm³. The allowed regions of the EoS's derived from the blue and red diamonds (former and latter pressures, respectively) are shown in the middle of the top row of Fig. 1 by the palish blue and yellow areas, in this order. The μ_H corresponding to these points are $\mu_H = 1014.5$ and 961.7 MeV, respectively.

Regarding interpolation between this later band and pQCD, the results of the case obtained without considering astrophysical constraints, to study dark matter as well as to test GR and beyond it, are displayed in the upper right side of Fig. 1, with the red area showing the corresponding band and taking into account possible PT for $n > 2.5n_s$. Grey and pale pink areas display integral constraints at pQCD for blue ($P = 4380 \text{ MeV/fm}^3$) and red circle ($P = 2330 \text{ MeV/fm}^3$), respectively. The second case used here is to consider astrophysical observables, six independent mass measurements at radius known, from the pulsars HESS J1731-34, PSR J0030+045 (two independent radius measurements), J0740+6620 (two independent radius measurements), PSR J0437-4715 and, as an upper bound, the mass of PSR J0952-0607, the heaviest NS observed. Applying the method of least squares, the band of EoS that minimizes χ^2 for the seven measurements is shown in the left side of the second row of Fig. 1, at the 68% CL (red area) and 95% CL (pink area). In the middle and in the right-hand side, Mass-Radius diagrams and Tidal deformability-Mass relations are displayed for the same bands. The band of EoS's obtained in this way also indicates possible PTs for NS masses $M \gtrsim 2.1 M_\odot$ at 68% CL, involving starting number densities above $2.5n_s$. We find both long and short coexistence regions during the PTs, corresponding to first and second order ones, respectively. Furthermore, this band also constraints the values of energy symmetry and its slope, with the resulting values $32.9 \leq S_0 \leq 39.5 \text{ MeV}$ and $37.3 \leq L \leq 69.0 \text{ MeV}$ at the 68% CL.

References

- [1] J. M. Alarcón and J. A. Oller, Phys. Rev. C **107** (2023) no.4, 044319.
- [2] E. L. Oter, A. Windisch, F. J. Llanes-Estrada and M. Alford, J. Phys. G **46** (2019) no.8, 084001.
- [3] E. Lope-Oter and F. J. Llanes-Estrada, Eur. Phys. J. A **58** (2022) no.1, 9
- [4] E. Lope-Oter and A. Wojnar, JCAP **02** (2024), 017. [
- [5] E. Lope-Oter and A. Wojnar, [arXiv:2402.03914 [gr-qc]].
- [6] E. Lope-Oter and F. J. Llanes-Estrada, Phys. Rev. C **105** (2022), L052801.
- [7] J. M. Alarcón, E. Lope-Oter and J. A. Oller, [arXiv:2410.14776 [nucl-th]].
- [8] O. Komoltsev and A. Kurkela, Phys. Rev. Lett. **128** (2022) no.20, 202701.
- [9] D. Adhikari *et al.* [PREX], Phys. Rev. Lett. **126** (2021) no.17, 172502.
- [10] D. Adhikari *et al.* [CREX], Phys. Rev. Lett. **129** (2022) no.4, 042501.
- [11] T. Gorda, A. Kurkela, *et al.* Phys. Rev. D **104** (2021) no.7, 074015.
- [12] B. T. Reed, F. J. Fattoyev, *et al.* Phys. Rev. Lett. **126** (2021) no.17, 172503.
- [13] B. T. Reed, F. J. Fattoyev, *et al.* Phys. Rev. C **109** (2024) no.3, 035803.
- [14] I. Tews, J. M. Lattimer, *et al.* Astrophys. J. **848** (2017) no.2, 105.
- [15] A. Lacour, J. A. Oller and U. G. Meißner, J. Phys. G **37** (2010), 125002.